THE JOURNAL OF PHYSICAL CHEMISTRY C

Article

Cite This: J. Phys. Chem. C 2019, 123, 8827−8835

pubs.acs.org/JPCC

# Nanoscale Friction on Confined Water Layers Intercalated between $MoS_2$ Flakes and Silica

Hyunsoo Lee,[†] Hochan Jeong,[‡] Joonki Suh,[∥,⊥] Won Hui Doh,[†] Jaeyoon Baik,[#] Hyun-Joon Shin,[#] Jae-Hyeon Ko,[‡] Junqiao Wu,[∥,⊥] Yong-Hyun Kim,*[,‡] and Jeong Young Park*[,†,§]

[†]Center for Nanomaterials and Chemical Reactions, Institute for Basic Science (IBS), Daejeon 34141, South Korea

[‡]Graduate School of Nanoscience and Technology and Department of Physics and [§]Graduate School of EEWS and Department of Chemistry, Korea Advanced Institute of Science and Technology (KAIST), Daejeon 34141, South Korea

[∥]Department of Materials Science and Engineering, University of California, Berkeley, California 94720, United States

[⊥]Materials Sciences Division, Lawrence Berkeley National Laboratory, Berkeley, California 94720, United States

[#]Pohang Accelerator Laboratory, Pohang University of Science and Technology, Pohang 37673, South Korea

Supporting Information

**ABSTRACT:** Frictional energy dissipation at the interfaces of two-dimensional (2D) materials through the excitation and transfer processes of kinetic energy into the bulk can be easily influenced by an intercalated water film. An enhancement of friction on water-intercalated graphene has been observed. Is this frictional enhancement by confined water a general phenomenon? We address this issue by investigating the frictional behavior of confined water layers intercalated between single-layer molybdenum disulfide ($MoS_2$), synthesized using chemical vapor deposition, and a silica substrate. The icelike water was intercalated by exposure to high-humidity air. We found that the intercalated water molecules morphologically deform the 2D $MoS_2$ sheet, forming distinct subdomains after the exposure to high humidity. We found that the adsorption of the icelike water layer between the $MoS_2$ and the silica leads to friction enhancement, compared with a pristine $MoS_2$/silica sample, which is associated with additional phononic friction energy dissipation at the solid−liquid interface, as indicated by the phonon distribution analysis from the empirical force-field calculations. Moreover, the atomic stick−slip behavior shows that the lattice orientation of the hydrophilic $MoS_2$ affects water molecule diffusion at the interface of the $MoS_2$/silica substrate. Chemical mapping of the water-intercalated $MoS_2$ on silica using scanning photoelectron microscopy and vacuum annealing processes shows water intercalation without changing the intrinsic composition of the $MoS_2$ on silica.

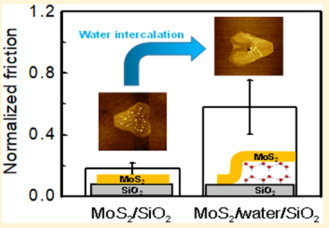


## 1. INTRODUCTION

Understanding mechanical kinetic energy dissipation in friction has drawn much attention in the physical sciences. Heat is the primary energy converted from the mechanical energy of sliding bodies in contact.[1−5] The processes of energy dissipation (e.g., molecular vibration of surface atoms,[3] chemical interactions,[6−8] electronic excitation with electron−hole coupling,[9] and stiffness[10,11]) contribute to friction phenomena at atomic scale. As a fundamental aspect of energy dissipation, it is important to understand the conversion of kinetic energy from sliding motion into the vibration of surface atoms. Coupling surface vibration with phonon modes of the substrate is also considered significant.[2] However, it is very difficult to experimentally investigate the origin of friction because of the complexity of the mechanism at the interface between bodies. Thus, a simple experimental design that provides a distinct main excitation mechanism for friction is necessary. In a previous report, we performed experimental and theoretical friction studies of graphene on mica with water layer intercalation as an antilubricant.[12,13] Since the hydrophobic graphene is transferred to the hydrophilic substrate (e.g., muscovite mica) using a mechanical method, the role of adsorbates from humid air at the interface of the graphene/mica is a highly important topic when studying surface behavior. The friction enhancement of graphene on mica by water layer intercalation and its isotope effects revealed that it is associated with phonon contributions.[12,13] In this confined water system, the hydrophobic graphene has very weak interaction with the intercalated water layer because of a lack of chemical bonds, whereas strong hydrogen bonds between the water layer and mica still occur. However, the generality of the role of confined water in friction remains an open question.

Hydrophilicity (i.e., an attraction to water molecules) plays a key role in the nanoscale tribological properties of 2D materials at ambient conditions. The Hertzian behavior of friction versus load curves depends on the humidity conditions during atomic force microscopy (AFM) measurements because of the effects of capillary condensation between the tip and the sample.[14−16] Gueye et al. demonstrated the relationship between friction, humidity, and temperature using AFM experiments and

Received: November 26, 2018
Revised: February 10, 2019
Published: March 12, 2019






DOI: 10.1021/acs.jpcc.8b11426
J. Phys. Chem. C 2019, 123, 8827−8835

proposed a 2D dynamic model.[17] The water layer between the tip and the sample leads to lower friction at low temperature and high humidity and decreases the van der Waals interaction between the tip and the sample during friction measurements. By confirming identical atomic stick−slip behavior of graphene in water and ultrahigh vacuum, Vilhena et al. suggested that friction experiments in water can be substituted for ultrahigh vacuum conditions.[18]

Molybdenum disulfide ($MoS_2$), a form of $MX_2$ (M: Mo, X: S) as a 2D transition metal dichalcogenide, consists of covalent bonds between the M and X in hexagonal arrangements.[19−24] The tribological properties of $MoS_2$ are very well known as lamellar solid lubricants.[25−29] The thickness dependence of $MoS_2$ on friction on a silica substrate was shown to be caused by puckering effects.[30] On mica, the friction coefficient of monolayer $MoS_2$ depends slightly on the relative humidity of the environment, compared with mica, because of its varied hydrophilicity.[15] In previous reports, the $MoS_2$ is intrinsically mildly hydrophilic, which was confirmed by Fourier-transform infrared spectroscopy and ellipsometry.[31,32] Another interesting characteristic of hydrophilic $MoS_2$ on a hydrophilic substrate is that the confined water layers are easily formed at interfaces.[33−36] A Stranski−Krastanov growth model was proposed for intercalated water molecules at the interfaces of hydrophobic graphene/mica, whereas water intercalated between hydrophilic $MoS_2$ and mica does not change because of the greater interactions between the layers.[32] Furthermore, Varghese et al. showed the effect of adsorbed water molecules between $MoS_2$ and mica on the optical properties of electron-doped $MoS_2$.[37] Thus, variable-environment hydrophilic 2D material systems provide an opportunity for understanding frictional energy dissipation and the role of adsorbates on morphological properties.

In this paper, we investigated the effects of water intercalated between hydrophilic $MoS_2$ and silica on friction against a Si tip using AFM. We found an enhancement of friction on $MoS_2$ on silica by water layer intercalation that is addressed by computational analysis. Both chemical mapping and vacuum annealing show the adsorption of a water layer at the interface of the $MoS_2$/silica through nonlocal transformation of the intrinsic composition of the $MoS_2$ before and after water intercalation. Furthermore, we found that the diffusion and growth of the water layer are associated with the lattice orientation of $MoS_2$ because of the relative interaction between the water layer and the $MoS_2$ sheet.

## 2. METHODS

**2.1. Sample Preparation and Characterization.** Monolayer $MoS_2$ was grown onto $SiO_2$/Si substrates using the ambient chemical vapor deposition (CVD) technique. Prior to CVD growth, the substrates were cleaned using a Piranha solution, a mixture of $H_2SO_4/H_2O_2$ (3:1), for 1 hour followed by deionized water rinsing and drying with $N_2$. The $MoO_3$ source (∼3 mg) was placed downstream from the sulfur source (∼1 g) and then heated to 700 °C for the growth step. The water intercalation treatments were performed in a glass cell (140 mm diameter, 150 mm height, and over 95% RH within several hours at room temperature (∼23 °C)) with deionized water. The RH was monitored using a digital thermo-hygrometer (RH measurements of 1 ∼ 99 ± 3% (TFA-GERMANY)). Vacuum annealing of the water-intercalated $MoS_2$ on silica was performed at 300 °C for 1 h at $10^{-9}$ Torr.

**2.2. Friction Force Microscopy (FFM) Measurements.** Friction force microscopy (FFM) measurements were performed at laboratory conditions (45−50% RH and 22−24 °C) using an environmental AFM (5500, Agilent). A Si tip (PPP-LFMR-50, Nanosensor) with a nominal resonance frequency of 23 kHz, cantilever thickness of 1.0 ± 1 μm, and force constant of 0.2 N/m was used for the FFM measurements of the water-intercalated $MoS_2$ sheet on silica. The friction was estimated by subtracting the retrace from the trace lateral signals during contact mode AFM measurements. A low normal load in the elastic regime was utilized for the friction measurements such that no damage occurred on the $MoS_2$ sample during the FFM experiments.

**2.3. Scanning Photoelectron Microscopy (SPEM) Measurements.** The X-ray was focused to a spatial resolution of about 200 nm using a Fresnel zone plate for the SPEM measurements and the photoelectron detector was positioned at a tilted angle of 54° to the surface normal direction, which indicated that the analytical probing depth became effectively as short as the topmost layers. The binding energies were calibrated using the Au 4f binding energy of an extra gold substrate. It was operated with a photon energy of 696.4 eV and an energy step of 0.8 eV. A binding energy of 284.8 eV for C 1s was used for the reference. The measurements were conducted at the beamline 8A1 at the Pohang Accelerator Laboratory in South Korea.

**2.4. Computational Method.** To calculate the $MoS_2$/water/$SiO_2$ structure, we used the slab model. In the first step, a (3 × 3 × 5) supercell of β-quartz $SiO_2$ ($a$ = 4.98 Å) was used for the substrate. To reduce lattice mismatch, we built a (5 × 5) $MoS_2$ monolayer (a = 3.09 Å) on a hydroxylated $SiO_2$(0001) surface. The model has a lattice mismatch of ∼3.4%. To consider the intercalation of an icelike water layer, we optimized 18 $H_2O$ molecules on the hydroxylated $SiO_2$(0001) surface. The surface of the $SiO_2$ substrate is terminated by hydroxyl groups (−OH) because of the RH conditions in the experiments.

Empirical interatomic potentials were used to describe the interactions between atoms, as implemented in the general utility lattice program (GULP).[38] To simulate the hydroxylated surface of the $SiO_2$, the CLAYFF force field[39] was adapted for Si−O and O−H. The simple point charge/flexible (q-SPC/Fw) potential was employed to explain the O−H bond in the $H_2O$ molecules.[40,41] For the Mo−S bond, we used the Stillinger−Weber potential.[42] The van der Waals interaction at each layer was evaluated using the Lennard-Jones (12−6) function.

$$E_{LJ}(r_{ij}) = \sum_{i \neq j} D_{ij}\left[\left(\frac{R_{ij}}{r_{ij}}\right)^{12} - 2\left(\frac{R_{ij}}{r_{ij}}\right)^{6}\right]$$

where $D_{ij}$ (kcal/mol) and $R_{ij}$ (Å) are empirical parameters. The parameters for Si, O, Mo, and S are listed in Table S1. The Lennard-Jones parameters between the different species were calculated using the arithmetic mean rule for $R_{ij}$ and the geometric mean rule for $D_{ij}$.

$$R_{ij} = \frac{1}{2}(R_i + R_j)$$

$$D_{ij} = \sqrt{D_i \times D_j}$$



DOI: 10.1021/acs.jpcc.8b11426
J. Phys. Chem. C 2019, 123, 8827−8835

## 3. RESULTS AND DISCUSSION

The synthesized single-layer $MoS_2$ (SL-$MoS_2$) was formed on a $SiO_2$ substrate with a thickness of 300 nm using the chemical vapor deposition (CVD) method.[43] The triangular structures of the SL-$MoS_2$ were very well defined in previous reports using high-resolution transmission electron microscopy[44] and scanning tunneling microscopy (STM).[45] The SL-$MoS_2$ on silica was characterized by photoluminescence (PL)[46] (Figure 1a) and Raman spectra[47] (Figure 1b) measurements. PL

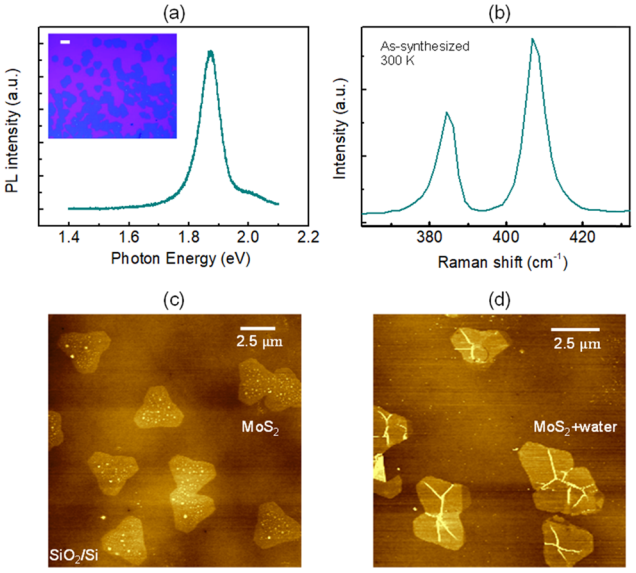


**Figure 1.** (a) Photoluminescence spectrum of the triangular single-crystal $MoS_2$ on silica. The inset is a large-area optical microscope image of the $MoS_2$ on silica, synthesized via chemical vapor deposition (CVD). Inset scale bar is 100 $\mu$m. (b) Raman spectra of pristine $MoS_2$ on silica acquired at ambient conditions. The two main peaks appearing at 384 and 407 $cm^{-1}$ are attributed to the in-plane ($^1E_{2g}$) and out-of-plane ($A_{1g}$) vibrations. Topography images of (c) CVD-synthesized triangular single-crystal pristine $MoS_2$ on $SiO_2$/Si and (d) $MoS_2$ on silica after exposure to high relative humidity (>90%) for several days.

spectra of a sample synthesized at 300 K show a very sharp major fluorescence feature at around 1.88 eV that originated from the direct band recombination of electron−hole pairs.[48] The Raman spectra show two different major peaks, which are associated with the in-plane ($^1E_{2g}$) and out-of-plane ($A_{1g}$) vibrations, appearing at 384 and 407 $cm^{-1}$, respectively.[47,48] Furthermore, we show the quality and crystallinity of the $MoS_2$ flakes using atomic stick−slip measurements[49] on the pristine $MoS_2$ sheet, which show clear sawtooth motions and lattice constants (3.2 Å) that are well matched with theoretical values (Figure S1). The triangular single-crystal $MoS_2$ on silica (i.e., we used the triangular structures with rounded corners from the $MoS_2$ growth process) is shown in the large-area topographical images that were acquired before (Figure 1c) and after (Figure 1d) water intercalation at ambient conditions with a relative humidity (RH) of 45−50% at room temperature. It shows uniform morphological changes caused by water intercalation. Since we need to consider the variation in height of the $MoS_2$ sheet on silica depending on the contact scanning conditions, the height of the SL-$MoS_2$ on $SiO_2$/Si is 0.8 ± 0.2 nm without water layer intercalation (0W), which is consistent with the value reported by Lee et al.[30]

We exposed the $MoS_2$ sample to high-RH conditions (i.e., above 99%) for several days (i.e., 117 h). Topography (Figure 2a) and friction (Figure 2b) images were simultaneously obtained at ambient conditions (~45% RH) before exposure. The cross sections along the red solid lines in topography and friction are shown in Figure 2c. In the topography, the small particles on $MoS_2$ flakes are visible. We suppose that these particles on the flakes are $MoS_2$ because of the lack of contrast in the friction image. Residues of $MoS_2$ particles can exist after chemical vapor deposition of $MoS_2$ flakes on silica. After exposure, topography (Figure 2d) and friction (Figure 2e) images of the $MoS_2$ sample were also obtained at ambient conditions. The labels correspond to (A) bare silica, (B) $MoS_2/SiO_2$, and (C) $MoS_2$/water/$SiO_2$. The wrinkles with heights of about 3−5 nm in the $MoS_2$ sheet bulging from the intercalated water molecules are clearly distinguished by the different heights in the line profiles (Figure 2f). The cross section along the red line in the topography image shows that two water layers are intercalated between the $MoS_2$ and $SiO_2$, as estimated by the height difference. The friction image clearly shows enhanced friction by water intercalation between the $MoS_2$ and $SiO_2$. Figure 2g shows a schematic diagram describing the cross-sectional view of intercalated water layers between $MoS_2$ and the $SiO_2$ substrate. The absolute value of the friction can be very sensitive to the scan conditions and the atmosphere between the tip and the sample (45−50% RH). Thus, we need to normalize the friction to compare the different images. The normalized friction behavior of $MoS_2$ in the presence of intercalated water layers between the $MoS_2$ sheet and silica is shown in Figure 2h. For this bar graph, the normalized friction value for $MoS_2$ + water was taken from the region marked with a solid red line in the friction image obtained after exposure. The friction was normalized using 1 as the maximum value of the $SiO_2$ friction. The friction enhancement on the $MoS_2$ with intercalated water layers is clearly seen as increased by a factor of ~3.2 above that on $MoS_2/SiO_2$. This result shows that the frictional energy dissipation of the 2D materials can be easily influenced by vibration of the intercalated water molecules at the interfaces. There are many $MoS_2$ flakes on the silica substrate after CVD synthesis. The flakes are simultaneously treated by exposure to high humidity on the silicon substrate. Figure 2 shows representative images of a $MoS_2$ flake on silica before and after water intercalation.

Another noteworthy finding is that the lattice orientation of single-crystal $MoS_2$ leads to the diffusion of adsorbed water molecules between the $MoS_2$ and the silica substrate. Topography (Figure 3a) and friction (Figure 3b) images of the water-intercalated $MoS_2$ on silica are shown after exposure to high RH for several days. The water-intercalated subdomain in the $MoS_2$ flake located in the center of the topography image has two straight lines that are parallel to each side of the $MoS_2$ triangle. The schematic diagram (Figure 3c) shows the areas of $MoS_2/SiO_2$ (yellow) and $MoS_2$/water/$SiO_2$ (blue), distinguished by their different heights. The dotted lines on each side of the triangular domains are shown using three colors that are indexed by the three different parallel directions. Since the single-crystal $MoS_2$ triangle is extremely well defined, the three sides of the triangular structure represent the lattice orientations of the $MoS_2$ flake. Thus, we can expect that the water-intercalated $MoS_2$ subdomain is related to the lattice orientation of the $MoS_2$. Moreover, the atomic stick−slip image measured on the $MoS_2$ plane (marked by the yellow


DOI: 10.1021/acs.jpcc.8b11426
J. Phys. Chem. C 2019, 123, 8827−8835

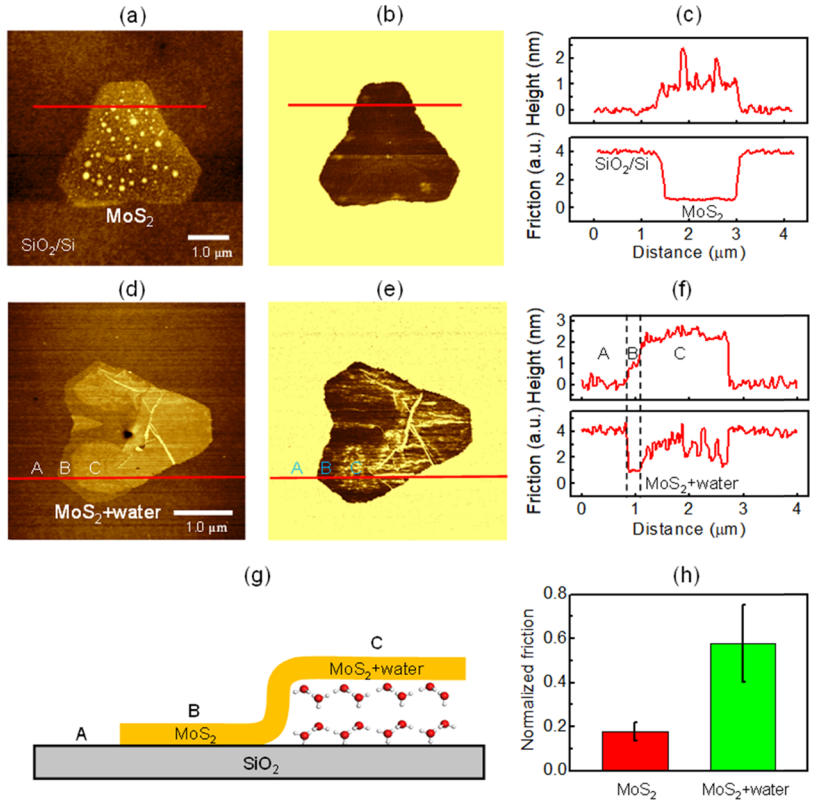


**Figure 2.** (a) Topography and (b) friction images (5.5 $\mu$m × 5.5 $\mu$m) of triangular single-crystal pristine $MoS_2$ on $SiO_2$/Si obtained in air at 45% RH with an applied force of 10 nN. (c) Line profiles of height (top) and friction (bottom) along the solid red lines in (a) and (b). After exposure of the $MoS_2$ on silica to high RH (>90%) for 117 h, (d) topography and (e) friction images (3.5 $\mu$m × 3.5 $\mu$m) of the water-intercalated $MoS_2$ on silica were acquired at ambient conditions. (f) Line profiles showing the height (top) and friction (bottom) of the regions with (labeled C) and without water intercalation (labeled B) between the $MoS_2$ and $SiO_2$ (labeled A) along the red lines in (d) and (e). (g) Schematic diagram describing the cross-sectional view of icelike water layers intercalated between SL-$MoS_2$ on a $SiO_2$ substrate along the red line in (d), (e), and (f). (h) Plot of the normalized friction (bare silica friction = 1) in accordance with presence of the water layers between $MoS_2$ and $SiO_2$.

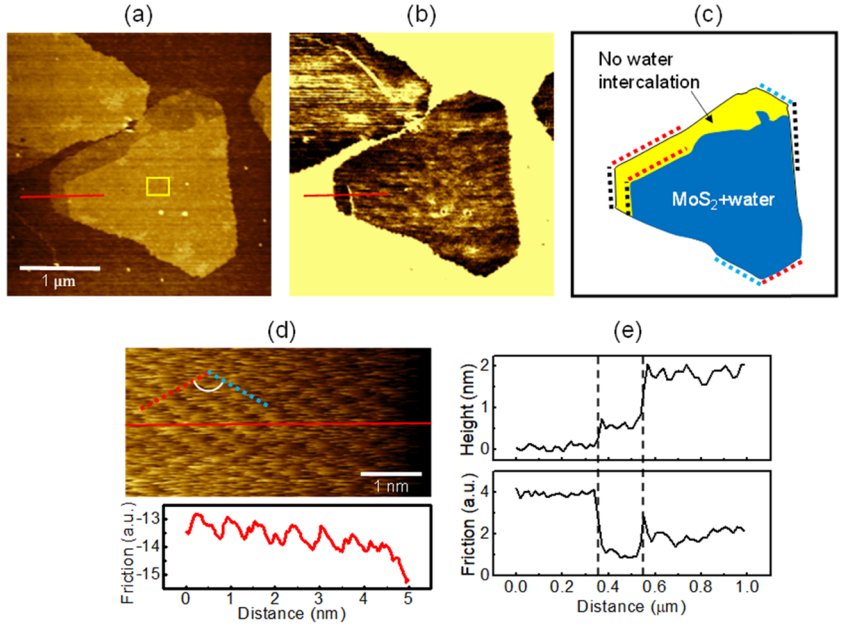


**Figure 3.** (a) Topography and (b) friction images (3.3 $\mu$m × 3.3 $\mu$m) of water-intercalated $MoS_2$ on a $SiO_2$/Si substrate after exposure to high RH (>90%) at an applied force of 10 nN. (c) Schematic diagram showing the shape and position of the water-intercalated areas between the $MoS_2$ sheet and silica, and three parallel sets of dotted edge guide lines with different colors (i.e., red, blue, and black). (d) Atomic stick–slip friction image (2.5 nm × 5.0 nm) on water-intercalated $MoS_2$ on silica and the sawtooth behavior of the AFM tip in cross-profile were obtained in the area marked by the yellow rectangle in (a). (e) Line profiles of height (top) and friction (bottom) along the solid red lines in (a) and (b).



DOI: 10.1021/acs.jpcc.8b11426
J. Phys. Chem. C 2019, 123, 8827–8835

rectangle in topography) shows that the edges of the intercalated water area depend on the lattice orientation of the $MoS_2$ (Figure 3d). The red and blue dotted lines in the schematic diagram show a 120° relation between the hexagonal arrangement of the elements in the stick−slip image. The line profile of the stick−slip also shows the sawtooth motion of the AFM cantilever on the $MoS_2$ surface. Therefore, the interaction between the hydrophilic 2D $MoS_2$ and the water layer plays an important role in determining the shape and diffusion of the intercalated water layer at the interfaces. Additional results showing that the edges of the water subdomain are aligned along the sides of $MoS_2$ flakes on silica are shown in the Supporting Information. Looking at water diffusion at the interface, Kim et al. reported that the diffusion pathways of the intercalated water follow the zigzag directions of the graphene on the substrate because the relative lower energy barrier for sliding occurs along the zigzag direction rather than other directions, as revealed by MD simulation.[50] The interaction between the $MoS_2$ sheet and the water layer also plays an important role in determining the shape and diffusion of the intercalated water layer at interfaces. Theoretical calculations of the potential energy of the intercalated water between $MoS_2$ and silica can be considered in a further study. The cross section along the red solid lines in the topography and friction images after water intercalation between the $MoS_2$ and $SiO_2$ are shown in Figure 3e.

To understand the effect of intercalated water on the friction on $MoS_2$, we examined the phonon density of states (DOS) of $MoS_2$ on a hydroxylated $SiO_2$ substrate with the form of $MoS_2/SiO_2$ and $MoS_2$/water/$SiO_2$. The phonon DOS was computed using the force-field approach, implemented in the general utility lattice program (GULP) (see the Computational Method section for details).[38] Figure 4 shows our calculation models, which are monolayer $MoS_2$ on a hydroxylated $SiO_2$ substrate with no water ($MoS_2/SiO_2$) (Figure 4a) and water intercalation ($MoS_2$/water/$SiO_2$) (Figure 4b). Our calculated structures are in good agreement with reported density function theory (DFT) results.[51−53] Figure 4c shows the partial phonon DOS of $MoS_2$ (top), water (middle), and $SiO_2$ (bottom) for $MoS_2/SiO_2$ (black solid line) and $MoS_2$/water/$SiO_2$ (blue solid line). The phonon DOS of the $MoS_2$ exists at 0−15 THz, the phonon DOS of intercalated water is distributed mainly between 0 and 30 THz, and the phonon DOS of the $SiO_2$ substrate is mainly present at 0−40 THz. In the presence of water layers, the phonon DOS of the water layers increases whereas the partial phonon DOS of $MoS_2$ and $SiO_2$ are almost unchanged because of the weak dispersion and hydrogen interactions between the water layers and the $MoS_2$ (or $SiO_2$) (Figure S2). The low interactions result from the intercalated water layer as an icelike structure that has a fully contacting H network from the water layer on a hydrophilic substrate, such as mica or silica.[54,55]

The intercalated water layers can increase the phonon excitation channels and the phonon DOS overlaps.[12] During tip−contact sliding, friction forces can excite atomic vibrations of both the monolayer $MoS_2$ and the water layers. Phonon excitation in the water layers provides additional excitation channels, thus enhancing the friction. The higher phonon DOS by water intercalation not only creates more phonon excitation but also increases the phonon DOS overlap between the $MoS_2$ and the $SiO_2$ substrate and between the water layers and the $SiO_2$ substrate. Because the frictional energy is mainly dissipated by transportation to the $SiO_2$ substrate through

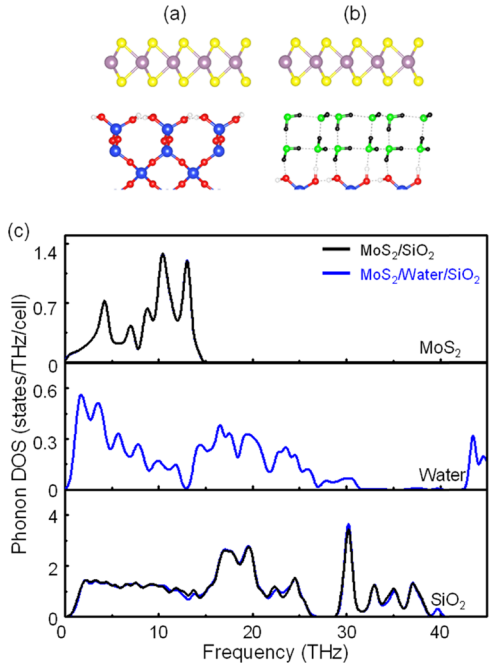


**Figure 4.** Side views of the optimized structures for monolayer $MoS_2$ on hydroxylated $\beta$-quartz $SiO_2$(0001) substrate with (a) no water and (b) with water layers. Atom representation: yellow (S), purple (Mo), white (H), red (O), blue (Si), black (H in $H_2O$), and green (O in $H_2O$). (c) Phonon DOS of monolayer $MoS_2$ on a hydroxylated $SiO_2$ substrate with no water (black) and water layers (blue). Projected phonon DOS of $MoS_2$ (top), water (middle), and $SiO_2$ (bottom) are shown for 0−45 THz.

the water layers, the increased phonon DOS overlap can contribute to enhanced frictional energy dissipation due to the presence of water layers. The directly excited phonon modes on the $MoS_2$ surface can dissipate by the phonon DOS overlap in the out-of-plane direction as well as via phonon−phonon scattering in the lateral direction. Therefore, when inserting water layers, the phonon modes of the water layers above 15 THz can be a potential channel for frictional energy dissipation by phonon−phonon scattering or anharmonic scattering.

Mechanical energy dissipation in friction from the 2D/water/bulk substrate model, such as our system of confined water between $MoS_2$ and silica, can thus be introduced by phonon contributions. In addition, other potential contributions to the frictional behavior of 2D materials can be considered (e.g., the puckering effect[30] and the true contact area between the tip and the surface[56]). The binding energy of the exciton as well as the electronic band gap of the $MoS_2$ sheet can also be intrinsically affected by the substrate. Again, we analyzed the friction at the same conditions with water intercalation between the $MoS_2$ and the $SiO_2$ substrate to exclude the intrinsic effect in the friction comparison. The intercalated water layer between a 2D thin film and a substrate can effectively screen the substrate charge-transfer effects.[13] Furthermore, the CVD-synthesized triangular single-layer $MoS_2$ is well known to have perfect crystallinity on the silica substrate. We also used this type of $MoS_2$ sample, as confirmed by PL, Raman spectroscopy, X-ray photoelectron spectroscopy (XPS), and atomic stick−slip measurements for the quality and crystallinity of the CVD $MoS_2$ flakes on the $SiO_2$ substrate. Thus, we can exclude any electrical effect from accidental doping of $MoS_2$ in our friction analysis. The influence of free



DOI: 10.1021/acs.jpcc.8b11426
J. Phys. Chem. C 2019, 123, 8827−8835

carriers in the probe was also ignored between the $MoS_2$ samples in our friction comparison in accordance with the confirmation of the stoichiometry of the $MoS_2$ on silica by XPS and SPEM. In particular, the atomic stick−slip behavior shows a pristine $MoS_2$ sheet without defect or lattice antisites, which clearly show the lattice constants (3.2 Å) as theoretical values. Thus, the structural defects of the $MoS_2$ sheet were not recognized by the characterization and it is also difficult to quantitatively present the density of defects. Additionally, the RMS roughness of the silica substrate is about 0.22 nm, which is definitely lower than the height of a single water layer (0.37 nm). Thus, the formation of intercalated water layers between $MoS_2$ and silica is clearly distinguished. When FFM is performed, the sharp AFM tip directly contacts the surface of the $MoS_2$ through any adsorbents on the $MoS_2$. Therefore, our friction results are not affected by adsorbents on the $MoS_2$ surface. The effect of lattice mismatch in our system is minor because any interaction between the $MoS_2$ and the water layers is a weak van der Waals interaction. In addition, the water structure is not well-ordered at room temperature, which leads to the absence of lattice mismatch after water intercalation.

Friction enhancement of $MoS_2$ on silica is observed across the whole area where the water layers are intercalated between the $MoS_2$ and the silica rather than on the edges of the $MoS_2$ flake. Thus, the effect of the edges of the $MoS_2$ in frictional variation is minor. However, the boundary of the water intercalation in a $MoS_2$ flake and the different average frictions between areas are clearly observed in the topography and friction images, as shown in Figure S3. Furthermore, in our study, the intercalated water layers that lead to friction enhancement of the $MoS_2$ by phonon contributions are formed between the $MoS_2$ and the silica; note that the relative humidity was consistently kept at about 45% during the friction measurements. This is a different experimental approach than that in the previous report that shows a frictional reduction with a fully formed ice layer between the tip and graphite at high relative humidity.[57] We note that the friction enhancement by water intercalation could be related to chemical bonds between the water and the $MoS_2$ and silica.

We confirmed that the height of the $MoS_2$ sheet on silica is reduced to values similar to those of pristine $MoS_2$ on silica and the subdomains were removed after vacuum annealing at 300 °C for 1 h at $10^{-9}$ Torr, which provides topographical evidence for water intercalation (Figure 5). Figure 5a shows a topographical image of a large area of water-intercalated SL-$MoS_2$ on a silica substrate after exposure to high-RH air for several days. After vacuum annealing, we can clearly confirm that the subdomain disappeared from the $MoS_2$ flakes on silica, although some wrinkles remained on the flakes in Figure 5b. The magnified image of one of the $MoS_2$ flakes on silica clearly shows that the subdomains vanished that originated from water layer intercalation and the edge alignments of the subdomain in Figure 5c. The line profile shows that the decreased height of the $MoS_2$ flake corresponds to the values of pristine SL-$MoS_2$ on silica before water intercalation, as shown in Figure 5d.

Furthermore, to confirm water intercalation between the $MoS_2$ and silica and the elements in the thin layer, we performed chemical analysis before and after vacuum annealing using SPEM[58] in beamline 8A1 at the Pohang Accelerator Laboratory. Figure 6 shows the SPEM results, which uses a Fresnel zone plate to focus the X-ray (spatial resolution about ~200 nm) on the triangular single-crystal $MoS_2$ on $SiO_2$ substrate with water intercalation. A photon energy of 696.4 eV was used. SPEM images (4.0 $\mu$m × 4.0 $\mu$m) and XPS spectra of S 2p (Figure 6a) and Mo 3d (Figure 6b) were obtained after water intercalation. The SPEM scan images were obtained with binding energies of 228.0−233.6 eV for Mo 3d and 159.4−165.0 eV for S 2p. The interval energy was 0.8 eV for imaging. The XPS spectra, which were measured on the

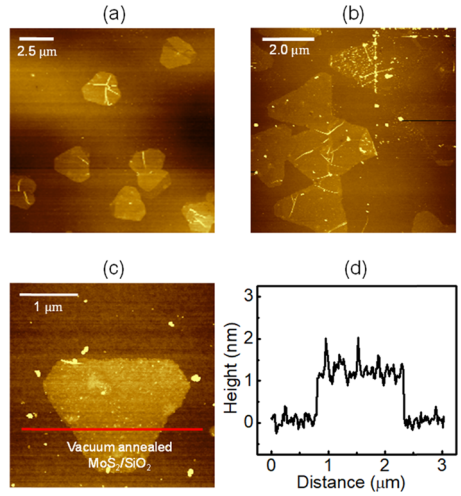


**Figure 5.** (a) Topography (15.0 $\mu$m × 15.0 $\mu$m) image before vacuum annealing of the water-intercalated $MoS_2$ on silica with regions containing $MoS_2/SiO_2$, $MoS_2$/water/$SiO_2$, and bare silica. (b) Topography (7.8 $\mu$m × 7.8 $\mu$m) and (c) magnified (3.3 $\mu$m × 3.3 $\mu$m) images after vacuum annealing of the water-intercalated $MoS_2$ on silica. (d) Line profile showing the height along the red line in (c) indicates that the intercalated water was removed by vacuum annealing.

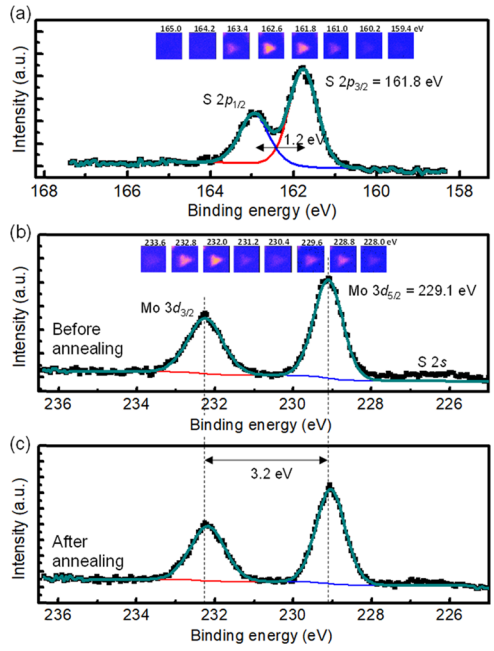


**Figure 6.** XPS spectra of (a) S 2p (S $2p_{1/2}$, S $2p_{3/2}$) and (b) Mo 3d (Mo $3d_{3/2}$, Mo $3d_{5/2}$) after water intercalation between the $MoS_2$ and silica that are identical to pristine $MoS_2$/silica. The insets are SPEM images acquired at each binding energy with an interval of 0.8 eV. The bright areas ($MoS_2$ flake) show higher intensity than the blue areas (bare $SiO_2$). (c) XPS spectra of Mo 3d on water-intercalated $MoS_2$ on silica after vacuum annealing.



DOI: 10.1021/acs.jpcc.8b11426
J. Phys. Chem. C 2019, 123, 8827−8835

$MoS_2$ sheet, each have two main peaks for S 2p (i.e., S $2p_{1/2}$, S $2p_{3/2}$) and Mo 3d (i.e., Mo $3d_{3/2}$, Mo $3d_{5/2}$). The binding energy of the S $2p_{3/2}$ and Mo $3d_{5/2}$ peaks are 161.8 and 229.1 eV, respectively, and each energy gap is 1.2 and 3.2 eV for the S 2p and Mo 3d, respectively, at 284.8 eV using C 1s as the reference, which are all consistent with values from the literature.[58,59] The bright contrast of the triangle shape in the SPEM images is clear at the peaks of the XPS spectra that identify the single-crystal $MoS_2$ on $SiO_2$ substrate. We thus confirm that there is no change in the Mo 3d and S 2p in the XPS spectra after water intercalation. The SPEM images also show the triangular equilibrium shape of the $MoS_2$ without local distortion, which means that the stoichiometry of the $MoS_2$ thin film is not influenced by water intercalation. In addition, molybdenum trioxide ($MoO_3$), which can be defined at binding energies of 233.15 and 236.28 eV as Mo $3d_{5/2}$ and Mo $3d_{3/2}$, respectively, was not detected before or after vacuum annealing of the water-intercalated $MoS_2$ on silica, as shown in Figure 6c. In this experiment, we performed the vacuum annealing of water-intercalated $MoS_2$ on silica at 300 °C for 1 h at $10^{-9}$ Torr to avoid any change in the $MoS_2$ sheet. In previous reports, Wu et al. revealed that there was no change in the $MoS_2$ sheet at annealing temperatures up to 300 °C.[60] It is effective to use the mechanical exfoliation method to clean the sample and remove any residue after the formation of $MoS_2$ on a substrate. On the other hand, thinning and decomposition of the $MoS_2$ sheet were revealed at temperatures above 330 °C, which is associated with oxidation to form $MoO_3$. Furthermore, Eda et al. show the change in the XPS spectra of Mo 3d as a function of annealing temperature from 50 to 300 °C and the $MoO_3$ feature was not present in the XPS spectra at temperatures up to 300 °C.[59] This is consistent with our measurements using the synchrotron XPS. The local inhomogeneity of the frictional contrast (e.g., the streaky feature in the friction image obtained after exposure on the water-intercalated $MoS_2$ flakes) could be associated with aspects of kinetic dynamics and instability of the water layers at the interface during the friction measurements. We note that the dynamic behavior of the water layers during the frictional measurement could be a very intriguing subject for a follow-up study.

## 4. CONCLUSIONS

In conclusion, we have found that water layers intercalated between $MoS_2$ and silica lead to friction enhancement of the $MoS_2$ sheet, compared with pristine $MoS_2$ on a silica substrate. Water intercalation without chemical transformation of the pristine $MoS_2$ on silica is confirmed by SPEM and vacuum annealing. We also demonstrate that the lattice orientation of hydrophilic $MoS_2$ leads to water molecule diffusion at the interface of the $MoS_2$/silica substrate. Phonon DOS analysis indicates that frictional enhancement by confined water is a general phenomenon that is associated with the direct excitation of vibrational energies of the $MoS_2$ and the confined water and the subsequent transfer to the bulk phonon modes of the substrate.

## ■ ASSOCIATED CONTENT

### Supporting Information

The Supporting Information is available free of charge on the ACS Publications website at DOI: 10.1021/acs.jpcc.8b11426.

Atomic stick−slip of $MoS_2$ on silica; phonon density of states of $MoS_2$, water, and $SiO_2$; parameters for the Lennard-Jones potentials for Si, O, Mo, and S; and topography and friction images of water-intercalated $MoS_2$ on silica (PDF)

## ■ AUTHOR INFORMATION


### Corresponding Authors

*E-mail: yong.hyun.kim@kaist.ac.kr (Y.H.K.).
*E-mail: jeongypark@kaist.ac.kr (J.Y.P.).

### ORCID

Junqiao Wu: 0000-0002-1498-0148
Yong-Hyun Kim: 0000-0003-4255-2068
Jeong Young Park: 0000-0002-8132-3076


### Notes

The authors declare no competing financial interest.

## ■ ACKNOWLEDGMENTS

This work was supported by the Institute for Basic Science (IBS) [IBS-R004]. H.J. and Y.-H.K. were supported by the National Research Foundation of Korea (2018R1A2A2A14079326) and the Science Research Center (2016R1A5A1008184) programs. The work done at U.C. Berkeley (materials preparation and characterization) was supported by US NSF Grant No. DMR-1708448.

## ■ REFERENCES


(1) Persson, B. N. *Sliding Friction: Physical Principles and Applications*; Springer Science & Business Media: New York, 2000; Vol. *1*.

(2) Park, J. Y.; Salmeron, M. Fundamental Aspects of Energy Dissipation in Friction. *Chem. Rev.* **2014**, *114*, 677−711.

(3) Cannara, R. J.; Brukman, M. J.; Cimatu, K.; Sumant, A. V.; Baldelli, S.; Carpick, R. W. Nanoscale Friction Varied by Isotopic Shifting of Surface Vibrational Frequencies. *Science* **2007**, *318*, 780−783.

(4) Park, J. Y.; Ogletree, D.; Thiel, P.; Salmeron, M. Electronic Control of Friction in Silicon Pn Junctions. *Science* **2006**, *313*, 186.

(5) Kisiel, M.; Gnecco, E.; Gysin, U.; Marot, L.; Rast, S.; Meyer, E. Suppression of Electronic Friction on Nb Films in the Superconducting State. *Nat. Mater.* **2011**, *10*, 119−122.

(6) Labuda, A.; Hausen, F.; Gosvami, N. N.; Grütter, P. H.; Lennox, R. B.; Bennewitz, R. Switching Atomic Friction by Electrochemical Oxidation. *Langmuir* **2011**, *27*, 2561−2566.

(7) Chen, J.; Ratera, I.; Park, J. Y.; Salmeron, M. Velocity Dependence of Friction and Hydrogen Bonding Effects. *Phys. Rev. Lett.* **2006**, *96*, No. 236102.

(8) Hausen, F.; Gosvami, N. N.; Bennewitz, R. Anion Adsorption and Atomic Friction on Au(111). *Electrochim. Acta* **2011**, *56*, 10694−10700.

(9) Filleter, T.; McChesney, J. L.; Bostwick, A.; Rotenberg, E.; Emtsev, K. V.; Seyller, T.; Horn, K.; Bennewitz, R. Friction and Dissipation in Epitaxial Graphene Films. *Phys. Rev. Lett.* **2009**, *102*, No. 086102.

(10) Kwon, S.; Ko, J.-H.; Jeon, K.-J.; Kim, Y.-H.; Park, J. Y. Enhanced Nanoscale Friction on Fluorinated Graphene. *Nano Lett.* **2012**, *12*, 6043−6048.

(11) Ko, J.-H.; Kwon, S.; Byun, I.-S.; Choi, J. S.; Park, B. H.; Kim, Y.-H.; Park, J. Y. Nanotribological Properties of Fluorinated, Hydrogenated, and Oxidized Graphenes. *Tribol. Lett.* **2013**, *50*, 137−144.

(12) Lee, H.; Ko, J.-H.; Choi, J. S.; Hwang, J. H.; Kim, Y.-H.; Salmeron, M.; Park, J. Y. Enhancement of Friction by Water Intercalated between Graphene and Mica. *J. Phys. Chem. Lett.* **2017**, *8*, 3482−3487.




DOI: 10.1021/acs.jpcc.8b11426
J. Phys. Chem. C 2019, 123, 8827−8835

(13) Lee, H.; Ko, J.-H.; Song, H. C.; Salmeron, M.; Kim, Y.-H.; Park, J. Y. Isotope- and Thickness-Dependent Friction of Water Layers Intercalated between Graphene and Mica. *Tribol. Lett.* **2018**, *66*, 36.
(14) Binggeli, M.; Mate, C. M. Influence of Capillary Condensation of Water on Nanotribology Studied by Force Microscopy. *Appl. Phys. Lett.* **1994**, *65*, 415−417.
(15) Schumacher, A.; Kruse, N.; Prins, R.; Meyer, E.; Lüthi, R.; Howald, L.; Güntherodt, H. J.; Scandella, L. Influence of Humidity on Friction Measurements of Supported $MoS_2$ Single Layers. *J. Vac. Sci. Technol. B* **1996**, *14*, 1264−1267.
(16) Gnecco, E.; Bennewitz, R.; Gyalog, T.; Meyer, E. Friction Experiments on the Nanometre Scale. *J. Phys.: Condens. Matter* **2001**, *13*, R619−R642.
(17) Gueye, B.; Zhang, Y.; Wang, Y.; Chen, Y. Experimental and Theoretical Investigations on the Nanoscale Kinetic Friction in Ambient Environmental Conditions. *Nano Lett.* **2015**, *15*, 4704−4712.
(18) Vilhena, J. G.; Pimentel, C.; Pedraz, P.; Luo, F.; Serena, P. A.; Pina, C. M.; Gnecco, E.; Pérez, R. Atomic-Scale Sliding Friction on Graphene in Water. *ACS Nano* **2016**, *10*, 4288−4293.
(19) Radisavljevic, B.; Radenovic, A.; Brivio, J.; Giacometti, V.; Kis, A. Single-Layer $MoS_2$ Transistors. *Nat. Nanotechnol.* **2011**, *6*, 147−150.
(20) Esmaeili-Rad, M. R.; Salahuddin, S. High Performance Molybdenum Disulfide Amorphous Silicon Heterojunction Photodetector. *Sci. Rep.* **2013**, *3*, No. 2345.
(21) Wang, Q. H.; Kalantar-Zadeh, K.; Kis, A.; Coleman, J. N.; Strano, M. S. Electronics and Optoelectronics of Two-Dimensional Transition Metal Dichalcogenides. *Nat. Nanotechnol.* **2012**, *7*, 699−712.
(22) Geim, A. K.; Grigorieva, I. V. Van Der Waals Heterostructures. *Nature* **2013**, *499*, 419−425.
(23) Chhowalla, M.; Shin, H. S.; Eda, G.; Li, L.-J.; Loh, K. P.; Zhang, H. The Chemistry of Two-Dimensional Layered Transition Metal Dichalcogenide Nanosheets. *Nat. Chem.* **2013**, *5*, 263−275.
(24) Mak, K. F.; Lee, C.; Hone, J.; Shan, J.; Heinz, T. F. Atomically Thin $MoS_2$: A New Direct-Gap Semiconductor. *Phys. Rev. Lett.* **2010**, *105*, No. 136805.
(25) Donnet, C.; Martin, J. M.; Le Mogne, T.; Belin, M. The Origin of Super-Low Friction Coefficient of $MoS_2$ Coatings in Various Environments. *Tribol. Ser.* **1994**, *27*, 277−284.
(26) Donnet, C.; Martin, J. M.; Le Mogne, T.; Belin, M. Super-Low Friction of $MoS_2$ Coatings in Various Environments. *Tribol. Int.* **1996**, *29*, 123−128.
(27) Xie, H.; Jiang, B.; He, J.; Xia, X.; Pan, F. Lubrication Performance of $MoS_2$ and $SiO_2$ Nanoparticles as Lubricant Additives in Magnesium Alloy-Steel Contacts. *Tribol. Int.* **2016**, *93*, 63−70.
(28) Chhowalla, M.; Amaratunga, G. A. J. Thin Films of Fullerene-Like $MoS_2$ Nanoparticles with Ultra-Low Friction and Wear. *Nature* **2000**, *407*, 164−167.
(29) Martin, J. M.; Donnet, C.; Le Mogne, T.; Epicier, T. Superlubricity of Molybdenum Disulphide. *Phys. Rev. B* **1993**, *48*, 10583−10586.
(30) Lee, C.; Li, Q.; Kalb, W.; Liu, X.-Z.; Berger, H.; Carpick, R. W.; Hone, J. Frictional Characteristics of Atomically Thin Sheets. *Science* **2010**, *328*, 76−80.
(31) Kozbial, A.; Gong, X.; Liu, H.; Li, L. Understanding the Intrinsic Water Wettability of Molybdenum Disulfide ($MoS_2$). *Langmuir* **2015**, *31*, 8429−8435.
(32) Song, J.; Li, Q.; Wang, X.; Li, J.; Zhang, S.; Kjems, J.; Besenbacher, F.; Dong, M. Evidence of Stranski−Krastanov Growth at the Initial Stage of Atmospheric Water Condensation. *Nat. Commun.* **2014**, *5*, No. 4837.
(33) Xu, K.; Cao, P.; Heath, J. R. Graphene Visualizes the First Water Adlayers on Mica at Ambient Conditions. *Science* **2010**, *329*, 1188−1191.
(34) Severin, N.; Lange, P.; Sokolov, I. M.; Rabe, J. P. Reversible Dewetting of a Molecularly Thin Fluid Water Film in a Soft Graphene−Mica Slit Pore. *Nano Lett.* **2012**, *12*, 774−779.
(35) Yasaei, P.; Bijandra, K.; Tara, F.; Canhui, W.; Mohammad, A.; David, T.; Ernesto, I. J.; Klie, R. F.; Amin, S.-K. High-Quality Black Phosphorus Atomic Layers by Liquid-Phase Exfoliation. *Adv. Mater.* **2015**, *27*, 1887−1892.
(36) Lee, M.; Choi, J.; Kim, J.-S.; Byun, I.-S.; Lee, D.; Ryu, S.; Lee, C.; Park, B. Characteristics and Effects of Diffused Water between Graphene and a $SiO_2$ Substrate. *Nano Res.* **2012**, *5*, 710−717.
(37) Varghese, J. O.; Agbo, P.; Sutherland, A. M.; Brar, V. W.; Rossman, G. R.; Gray, H. B.; Heath, J. R. The Influence of Water on the Optical Properties of Single-Layer Molybdenum Disulfide. *Adv. Mater.* **2015**, *27*, 2734−2740.
(38) Gale, J. D.; Rohl, A. L. The General Utility Lattice Program (Gulp). *Mol. Simul.* **2003**, *29*, 291−341.
(39) Cygan, R. T.; Liang, J.-J.; Kalinichev, A. G. Molecular Models of Hydroxide, Oxyhydroxide, and Clay Phases and the Development of a General Force Field. *J. Phys. Chem. B* **2004**, *108*, 1255−1266.
(40) Paesani, F.; Zhang, W.; Case, D. A.; Cheatham, T. E.; Voth, G. A. An Accurate and Simple Quantum Model for Liquid Water. *J. Chem. Phys.* **2006**, *125*, No. 184507.
(41) Wu, Y.; Tepper, H. L.; Voth, G. A. Flexible Simple Point-Charge Water Model with Improved Liquid-State Properties. *J. Chem. Phys.* **2006**, *124*, No. 024503.
(42) Jiang, J.-W.; Park, H. S.; Rabczuk, T. Molecular Dynamics Simulations of Single-Layer Molybdenum Disulphide ($MoS_2$): Stillinger-Weber Parametrization, Mechanical Properties, and Thermal Conductivity. *J. Appl. Phys.* **2013**, *114*, No. 064307.
(43) Tongay, S.; Fan, W.; Kang, J.; Park, J.; Koldemir, U.; Suh, J.; Narang, D. S.; Liu, K.; Ji, J.; Li, J.; et al. Tuning Interlayer Coupling in Large-Area Heterostructures with CVD-Grown $MoS_2$ and $WS_2$ Monolayers. *Nano Lett.* **2014**, *14*, 3185−3190.
(44) van der Zande, A. M.; Huang, P. Y.; Chenet, D. A.; Berkelbach, T. C.; You, Y.; Lee, G.-H.; Heinz, T. F.; Reichman, D. R.; Muller, D. A.; Hone, J. C. Grains and Grain Boundaries in Highly Crystalline Monolayer Molybdenum Disulphide. *Nat. Mater.* **2013**, *12*, 554−561.
(45) Tuxen, A.; Kibsgaard, J.; Gøbel, H.; Lægsgaard, E.; Topsøe, H.; Lauritsen, J. V.; Besenbacher, F. Size Threshold in the Dibenzothiophene Adsorption on $MoS_2$ Nanoclusters. *ACS Nano* **2010**, *4*, 4677−4682.
(46) Splendiani, A.; Sun, L.; Zhang, Y.; Li, T.; Kim, J.; Chim, C.-Y.; Galli, G.; Wang, F. Emerging Photoluminescence in Monolayer $MoS_2$. *Nano Lett.* **2010**, *10*, 1271−1275.
(47) Li, H.; Zhang, Q.; Yap, C. C. R.; Tay, B. K.; Edwin, T. H. T.; Olivier, A.; Baillargeat, D. From Bulk to Monolayer $MoS_2$: Evolution of Raman Scattering. *Adv. Funct. Mater.* **2012**, *22*, 1385−1390.
(48) Yin, Z.; Li, H.; Li, H.; Jiang, L.; Shi, Y.; Sun, Y.; Lu, G.; Zhang, Q.; Chen, X.; Zhang, H. Single-Layer $MoS_2$ Phototransistors. *ACS Nano* **2012**, *6*, 74−80.
(49) Lee, H.; Qi, Y.; Kwon, S.; Salmeron, M.; Park, J. Y. Large Changes of Graphene Conductance as a Function of Lattice Orientation between Stacked Layers. *Nanotechnology* **2015**, *26*, No. 015702.
(50) Kim, J.-S.; Choi, J. S.; Lee, M. J.; Park, B. H.; Bukhvalov, D.; Son, Y.-W.; Yoon, D.; Cheong, H.; Yun, J.-N.; Jung, Y.; et al. Between Scylla and Charybdis: Hydrophobic Graphene-Guided Water Diffusion on Hydrophilic Substrates. *Sci. Rep.* **2013**, *3*, No. 2309.
(51) Dolui, K.; Rungger, I.; Sanvito, S. Origin of the N-Type and P-Type Conductivity of $MoS_2$ Monolayers on a $SiO_2$ Substrate. *Phys. Rev. B* **2013**, *87*, No. 165402.
(52) Chen, Y.-W.; Cheng, H.-P. Structure and Stability of Thin Water Films on Quartz Surfaces. *Appl. Phys. Lett.* **2010**, *97*, No. 161909.
(53) Gao, W.; Xiao, P.; Henkelman, G.; Liechti, K. M.; Huang, R. Interfacial Adhesion between Graphene and Silicon Dioxide by Density Functional Theory with Van Der Waals Corrections. *J. Phys. D: Appl. Phys.* **2014**, *47*, No. 255301.
(54) Li, H.; Zeng, X. C. Two Dimensional Epitaxial Water Adlayer on Mica with Graphene Coating: An Ab Initio Molecular Dynamics Study. *J. Chem. Theory Comput.* **2012**, *8*, 3034−3043.


DOI: 10.1021/acs.jpcc.8b11426
*J. Phys. Chem. C* 2019, 123, 8827−8835

(55) Odelius, M.; Bernasconi, M.; Parrinello, M. Two Dimensional Ice Adsorbed on Mica Surface. *Phys. Rev. Lett.* **1997**, *78*, 2855−2858.
(56) Li, S.; Li, Q.; Carpick, R. W.; Gumbsch, P.; Liu, X. Z.; Ding, X.; Sun, J.; Li, J. The Evolving Quality of Frictional Contact with Graphene. *Nature* **2016**, *539*, 541−545.
(57) Hasz, K.; Ye, Z.; Martini, A.; Carpick, R. W. Experiments and Simulations of the Humidity Dependence of Friction between Nanoasperities and Graphite: The role of Interfacial Contact Quality. *Phys. Rev. Mater.* **2018**, *2*, No. 126001.
(58) Park, W.; Baik, J.; Kim, T.-Y.; Cho, K.; Hong, W.-K.; Shin, H.-J.; Lee, T. Photoelectron Spectroscopic Imaging and Device Applications of Large-Area Patternable Single-Layer $MoS_2$ Synthesized by Chemical Vapor Deposition. *ACS Nano* **2014**, *8*, 4961−4968.
(59) Eda, G.; Yamaguchi, H.; Voiry, D.; Fujita, T.; Chen, M.; Chhowalla, M. Photoluminescence from Chemically Exfoliated $MoS_2$. *Nano Lett.* **2011**, *11*, 5111−5116.
(60) Wu, J.; Li, H.; Yin, Z.; Li, H.; Liu, J.; Cao, X.; Zhang, Q.; Zhang, H. Layer Thinning and Etching of Mechanically Exfoliated $MoS_2$ Nanosheets by Thermal Annealing in Air. *Small* **2013**, *9*, 3314−3319.



DOI: 10.1021/acs.jpcc.8b11426
*J. Phys. Chem. C* 2019, 123, 8827−8835